ACES JOURNAL, Vol. 35, No. 3, March 2020

Application of Barycentric Subdivision Method for Singularity Integration in Method of Moments

Chunwang Xiang [1], Xunwang Dang [2], Maokun Li [1*], Fan Yang [1], and Shenheng Xu [1]

[1] Department of Electronic Engineering
Tsinghua University, Beijing 100084, China
State Key Laboratory on Microwave and Digital Communications
Beijing National Research Center for Information Science and Technology (BNRist)
maokunli@tsinghua.edu.cn

[2] Science and Technology on Electromagnetic
Scattering Laboratory, Beijing 100854, China

Abstract ─ Method of moments (MoM) is an essential tool to model electromagnetic wave interactions with three-dimensional targets. Numerical integration is a key technique in MoM. Due to the singular nature of Green's function, MoM requires special treatment in the calculation of singular integration, which is usually time-consuming. In this study, the barycentric subdivision method is investigated to compute numerical integration in three-dimensional surface integral equations. This method allows a uniform treatment for both singular and non-singular integrals. Numerical examples show that this method could reach the same level of accuracy as the singularity extraction method for RWG basis functions, and the computational time of setting up the matrix can be reduced by half.

Index Terms ─ Barycentric subdivision method, Method of moments (MoM), Rao-Wilton-Glisson (RWG) basis, singular integration, singularity extraction method.

I. INTRODUCTION

Rao-Wilton-Glisson (RWG) basis [1] has been widely used in Method of Moments (MoM) for modeling electromagnetic wave interactions with 3D targets. While setting up the matrix equation of MoM, we usually use numerical integration to evaluate the source integrals and field integrals, both of which contain the Green's function. Because of the singular nature of the Green's function, the integrals need to be treated carefully when the domain of the source integral overlaps with the one of the field integrals. The commonly used techniques include singularity extraction [1,2], Duffy coordinate transformation [3-5], polar co-ordinate transformation, and etc.

The singularity extraction method was proposed by Wilton et al. [1]. This method evaluates the non-singular part of the integral by numerical quadrature and the singular part by analytical formula [2]. Khayat and Wilton proposed a simple and efficient numerical procedure, which uses singularity cancellation scheme [6]. Khayat et al. further optimized this method for the integration scheme [7]. Vipiana and Wilton presented a purely numerical procedure to evaluate strongly near-singular integrals in the gradient of Helmholtz-type potentials for observation points at small distances from the source domain [8]. Popovic [9], Geng and Tong [10, 11] also applied potential integral method to computing singular integrals based on bilinear surface modeling. Wang and Nie et al. used the singularity transferring method to calculate the integral with 1/R singularity in its integrand and remove the small area, which makes zero contribution to the numerical integration [12]. Hua and Xu reduced the order of singularity and avoided the coincidences between the source and field points [13]. Wu et al. extracted the strong singularity of Magnetic Field Integral Equation (MFIE) and used the integral domain transform to eliminate the residual mild singularity [14]. Vipiana and Wilton presented a simple and efficient numerical procedure for evaluating singular and near-singular source vector potential integrals involving junction basis functions based on a double transformation, which could cancel singularities [22]. Jarvenpaa presented recursive formulas by which they can extract any number of terms from the singular kernel and generalize the singularity extraction technique for surface and volume integral equation with high-order basis functions [23]. These methods can compute the singular integral with good accuracy. However, we have to carefully separate the singular and non-singular integral so that they can be treated differently. Also, compared with non-singular integrals, the singular integrals are more expensive to compute. It can become

Submitted On: March 21, 2019
Accepted On: September 7, 2019

1054-4887 © ACES

a bottleneck in computing time for method of moments.

The Duffy coordinate transform method was proposed by Duffy [3]. This is a simple transformation that facilitates the evaluation of integrals with singular integrands at a vertex. Zhao and Nie et al. used domain decomposition and Duffy coordinate transformation to remove the singularity in the integrand [4]. Botha presented a new family of systematically constructed near-singularity cancellation transformations, which yields quadrature rules for integrating near-singular kernels over triangular surfaces based on Duffy transformation [5]. Zhang and Sun constructed a general variable transformation based on the idea of diminishing the difference of the orders of magnitude, which can remove the near singularity efficiently by eliminating the rapid variations of the integrand in nearly singular integrals, and improve the accuracy of numerical results [23]. Duffy transformation eliminates the singularity in the integral through coordinate transformation and evaluates the integral numerically. But the non-singular and singular integrations are still treated separately. Besides, the errors of the numerical quadrature would increase for triangles with small aspect ratios. Because Duffy transformation requires coordinate transform and computation of quadrature points, fast evaluation of the singular integrals is still a challenge.

In this work, we studied the barycentric subdivision method, which is also known as the nine-point numerical integration, for computing integrals in MoM. It was originally applied to image rendering in computer science [15]. Makarov introduced the method into RWG-MoM [16], and he stated in his works that this technique was not very accurate. Hence, this method has not been widely used. Xiang et al. also studied this method in 2017 [21]. In this method, the singular integrals are evaluated in the same fashion as the non-singular ones, which allows a uniform treatment of the numerical integrals. Therefore, the time of setting up the MoM matrix equation can be reduced. Numerical examples showed that the accuracy is still in remained in the results.

Compared with [16], more details of the barycentric method are studied in this paper, especially its numerical accuracy, which is compared with one of the singularity extraction schemes. The accuracy is important in the application of the scheme for solving electromagnetic problems. Based on both derivation and numerical examples, we found that the accuracy of this scheme is comparable to the singularity extraction scheme. A more detailed convergence analysis of the numerical accuracy of this scheme is presented. It is proved that the integral will converge when the triangle gets smaller, similar as other integration schemes. This scheme is only applied to EIFE in reference [16], we also investigated its applicability for MFIE, PMCHWT and FEM-BI formulations. It seems to work as well.

This paper is organized as follows: Section II describes the formulation. In Section III, numerical examples are given to show the efficiency and accuracy of this method. In Section IV, a convergence analysis is carried out. Section V summarizes this work.

II. FORMULATION

A. Electric field integral equation (EFIE) for PEC targets

The electric field on the surface of a perfect electric conductor (PEC) target satisfies the following integral equation [17, 18]:

$$\hat{n} \times \overline{\overline{L}}(\bar{\mathbf{J}}) = \hat{n} \times \mathbf{E}^{inc}(\mathbf{r}), \mathbf{r} \in S_0, \tag{1}$$

where

$$\overline{\overline{L}}(\bar{\mathbf{J}}) = jk_0 \iint_{S_0} \bar{\mathbf{J}}(\mathbf{r}')G(\mathbf{r},\mathbf{r}')dS' + \frac{j}{k_0}\iint_{S_0} \nabla' \cdot \bar{\mathbf{J}}(\mathbf{r}')\nabla G(\mathbf{r},\mathbf{r}')dS', \tag{2}$$

where G(**r**,**r**') denotes the Green's function in free space, $\bar{\mathbf{J}}$ denotes the scaled electric current density on the surface of the target. Discretizing $\bar{\mathbf{J}}$ by RWG basis and applying the Galerkin's method, we can setup a matrix of MoM with elements as [18]:

$$Z_{mn} = jk_0 \iint_{S_0} \mathbf{f}_m(\mathbf{r}) \cdot \left[\iint_{S_0} \mathbf{f}_n(\mathbf{r}')G(\mathbf{r},\mathbf{r}')dS'\right]dS - \frac{j}{k_0}\iint_{S_0} \nabla \cdot \mathbf{f}_m(\mathbf{r})\left[\iint_{S_0} \nabla' \cdot \mathbf{f}_n(\mathbf{r}')G(\mathbf{r},\mathbf{r}')dS'\right]dS, \tag{3}$$

where Z_{mn} represents the electric field generated by the *n-th* basis function and tested by the *m-th* basis function. $\boldsymbol{f}_m(\mathbf{r})$ and $\boldsymbol{f}_n(\mathbf{r})$ represent the RWG basis functions, which can be written as:

$$\mathbf{f}_m(\mathbf{r}) = \begin{cases} \dfrac{l_n}{2A_m^+}\boldsymbol{\rho}_m^+(\mathbf{r}), \mathbf{r}\ in\ \mathrm{T}_m^+ \\ \dfrac{l_n}{2A_m^-}\boldsymbol{\rho}_m^-(\mathbf{r}), \mathbf{r}\ in\ \mathrm{T}_m^- \\ 0, \quad otherwise \end{cases}, \tag{4}$$

where $\mathrm{T}_m^{\pm}$ denote the two triangles associated with the *m-th* edge, $\mathrm{A}_m^{\pm}$ are the areas of triangles $\mathrm{T}_m^{\pm}$, and $\rho_m^{\pm}$ are the vectors defined in Fig. 1, other symbols are the same as those in reference [1].

The integral in Eq. (3) then becomes:

$$Z_{mn} = jk_0\frac{l_m}{2A_m^+}\iint_{T_m^+}(\mathbf{r}-\mathbf{r}_i)\cdot\tilde{\mathbf{A}}[\mathbf{r}, f_n(\mathbf{r}')]dS + jk_0\frac{l_m}{2A_m^-}\iint_{T_m^-}(\mathbf{r}_j-\mathbf{r})\cdot\tilde{\mathbf{A}}[\mathbf{r}, f_n(\mathbf{r}')]dS - \frac{jl_m}{k_0A_m^+}\iint_{T_m^+}\tilde{\Phi}[\mathbf{r}, f_n(\mathbf{r}')]dS + \frac{jl_m}{k_0A_m^-}\iint_{T_m^-}\tilde{\Phi}[\mathbf{r}, f_n(\mathbf{r}')]dS, \tag{5}$$

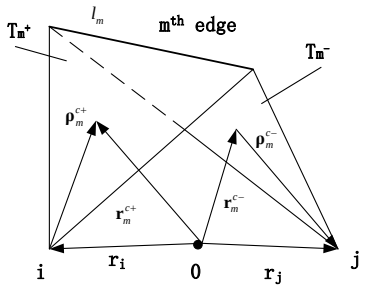

Fig. 1. RWG basis function defined on the *m-th* edge.

In this method, we can use one-point quadrature for the field integral. The barycenter of the *m-th* triangle elements is chosen as the testing point. The matrix element $\mathbf{Z}_{mn}$ can then be written as:

$$\begin{aligned} \mathbf{Z}_{mn} &= jk_0 \frac{l_m}{2}(\mathbf{r}_m^{c+} - \mathbf{r}_i)\cdot\tilde{\mathbf{A}}[\mathbf{r}_m^{c+}, f_n(\mathbf{r}')] \\ &+ jk_0 \frac{l_m}{2}(\mathbf{r}_j - \mathbf{r}_m^{c-})\cdot\tilde{\mathbf{A}}[\mathbf{r}_m^{c-}, f_n(\mathbf{r}')] \\ &- \frac{jl_m}{k_0}\tilde{\Phi}\left[\mathbf{r}_m^{c+}, f_n(\mathbf{r}')\right] + \frac{jl_m}{k_0}\tilde{\Phi}\left[\mathbf{r}_m^{c-}, f_n(\mathbf{r}')\right]. \end{aligned} \quad (6)$$

Here $\mathbf{r}_m^{c\pm}$ is the barycenter of triangle in the *m-th* basis function, $\tilde{\mathbf{A}}$ and $\tilde{\Phi}$ represent the source integrals, which can be written as:

$$\begin{aligned} \tilde{\mathbf{A}}[\mathbf{r}, f_n(\mathbf{r}')] &= \frac{1}{4\pi}\frac{l_n}{2A_n^+}\iint_{T_n^+}(\mathbf{r}' - \mathbf{r}_i')\frac{e^{-jk_0R}}{R}dS' \\ &+ \frac{1}{4\pi}\frac{l_n}{2A_n^-}\iint_{T_n^-}(\mathbf{r}_j' - \mathbf{r}')\frac{e^{-jk_0R}}{R}dS', \end{aligned} \quad (7)$$

$$\tilde{\Phi}\left[\mathbf{r}, f_n(\mathbf{r}')\right] = \frac{1}{4\pi}\frac{l_n}{A_n^+}\iint_{T_n^+}\frac{e^{-jk_0R}}{R}dS' - \frac{1}{4\pi}\frac{l_n}{A_n^-}\iint_{T_n^-}\frac{e^{-jk_0R}}{R}dS', \quad (8)$$

where $R = |\mathbf{r} - \mathbf{r}'|$. The source integration in the *n-th* patch can be calculated by the barycentric subdivision method.

B. Magnetic field integral equation (MFIE) for PEC targets

The magnetic field on the surface of a perfect electric conductor (PEC) target satisfies the following integral equation [17, 18]:

$$\frac{1}{2}\bar{\mathbf{J}} + \hat{n}\times\bar{\bar{K}}(\bar{\mathbf{J}}) = \hat{n}\times\mathbf{H}^{inc}(\mathbf{r}), \mathbf{r}\in S_0, \quad (9)$$

where $\bar{\bar{K}}(\bar{\mathbf{J}}) = \oint\!\!\!\!\!\!\iint_{S_0}\bar{\mathbf{J}}(\mathbf{r}')\times\nabla G(\mathbf{r},\mathbf{r}')dS'$. Using the same method as EFIE, we can get the impedance matrix elements for MFIE as:

$$\begin{aligned} \mathbf{Z}_{mn} &= \frac{1}{2}\oint\!\!\!\!\!\!\iint_{S_0}\mathbf{f}_m(\mathbf{r})\cdot\mathbf{f}_n(\mathbf{r}')dS \\ &+ \oint\!\!\!\!\!\!\iint_{S_0}\mathbf{f}_m(\mathbf{r})\cdot\left[\hat{n}\times\oint\!\!\!\!\!\!\iint_{S_0}\mathbf{f}_n(\mathbf{r}')\times\nabla G(\mathbf{r},\mathbf{r}')dS'\right]dS, \end{aligned} \quad (10)$$

here, $\nabla G(\mathbf{r},\mathbf{r}') = (-jk_0 - \frac{1}{R})\frac{e^{-jk_0R}}{4\pi R^2}\mathbf{R}$.

Now the source integral for the singular point is extracted for separate analysis. We defined the $\mathbf{H}_i(r)$ as:

$$\begin{aligned} \mathbf{H}_i(\mathbf{r}) &= \oint\!\!\!\!\!\!\iint_{S_0}\mathbf{f}_n(\mathbf{r}')\times\nabla G(\mathbf{r},\mathbf{r}')dS' \\ &= -\frac{1}{2A_n}\oint\!\!\!\!\!\!\iint_{S_0}(-jk_0 - \frac{1}{R})\frac{e^{-jk_0R}}{4\pi R^2}\mathbf{R}\times\boldsymbol{\rho}_i'dS'. \end{aligned} \quad (11)$$

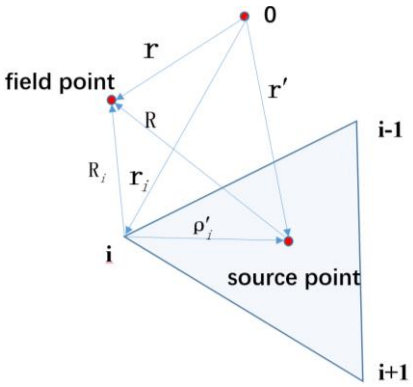

Fig. 2. The related vector and scalar location relationship between the field point and the source point coordination.

Figure 2 depicts the geometric relationship between the vector and the scalar, which are involved in the formula; substituting $\mathbf{R} = \mathbf{R}_i - \boldsymbol{\rho}_i'$ into equation (11), which will take the cross product out of the integral. Equation (11) can be written as:

$$\mathbf{H}_i(\mathbf{r}) = \frac{1}{2A_n}\mathbf{R}_i\times\oint\!\!\!\!\!\!\iint_{S_0}(jk_0 + \frac{1}{R})\frac{e^{-jk_0R}}{4\pi R^2}\boldsymbol{\rho}_i'dS'.$$

The integral of impedance matrix element, which is related to the *m-th* and *n-th* edges, can be written as:

$$\begin{aligned} Z_{mn} &= I_0(m^+, n) + I_0(m^-, n) \\ &+ \frac{l_m}{2A_m^+}\iint_{T_m^+}(\mathbf{r} - \mathbf{r}_i)\cdot\tilde{\mathbf{V}}[\mathbf{r}, f_n(\mathbf{r}')]dS \\ &+ \frac{l_m}{2A_m^-}\iint_{T_m^-}(\mathbf{r}_j - \mathbf{r})\cdot\tilde{\mathbf{V}}[\mathbf{r}, f_n(\mathbf{r}')]dS, \end{aligned} \quad (12)$$

where,

$$I_0(m^+, n) = \begin{cases} \frac{l_m l_n}{8A_n^+}(\mathbf{r}_m^{c+} - \mathbf{r}_i)\cdot(\mathbf{r}_n^{c+} - \mathbf{r}_i'), \mathbf{r}_m^{c+}\in T_n^+ \\ \frac{l_m l_n}{8A_n^-}(\mathbf{r}_m^{c+} - \mathbf{r}_i)\cdot(\mathbf{r}_j' - \mathbf{r}_n^{c-}), \mathbf{r}_m^{c+}\in T_n^- \\ 0, \quad otherwise \end{cases}, \quad (13)$$

$$I_0(m^-, n) = \begin{cases} \frac{l_m l_n}{8A_n^+}(\mathbf{r}_j - \mathbf{r}_m^{c-})\cdot(\mathbf{r}_n^{c+} - \mathbf{r}_i'), \mathbf{r}_m^{c-}\in T_n^+ \\ \frac{l_m l_n}{8A_n^-}(\mathbf{r}_j - \mathbf{r}_m^{c-})\cdot(\mathbf{r}_j' - \mathbf{r}_n^{c-}), \mathbf{r}_m^{c-}\in T_n^- \\ 0, \quad otherwise \end{cases}, \quad (14)$$

$$\begin{aligned} \tilde{\mathbf{V}}[\mathbf{r}, f_n(\mathbf{r}')] &= \frac{l_n}{2A_n^+}\hat{n}_m\times(\mathbf{r} - \mathbf{r}_i')\times\iint_{T_n^+}(\mathbf{r}' - \mathbf{r}_i')(jk_0 + \frac{1}{R})\frac{e^{-jkR}}{4\pi R^2}dS' \\ &+ \frac{l_n}{2A_n^-}\hat{n}_m\times(\mathbf{r} - \mathbf{r}_j')\times\iint_{T_n^-}(\mathbf{r}_j' - \mathbf{r}')(jk_0 + \frac{1}{R})\frac{e^{-jkR}}{4\pi R^2}dS', \end{aligned} \quad (15)$$

here, $\hat{n}_m$ is the outer normal on the patch of the *m-th* edge.

After using the one-point quadrature for the field integral about $\mathbf{r}$, the matrix element $\mathbf{Z}_{mn}$ can be written as:

$$\begin{aligned} Z_{mn} &= I_0(m^+, n) + I_0(m^-, n) \\ &+ \frac{l_m l_n}{16\pi A_n^+}(\mathbf{r}_m^{c+} - \mathbf{r}_i)\cdot\hat{n}_m \times (\mathbf{r}_m^{c+} - \mathbf{r}_i') \times \iint_{T_n^+}(\mathbf{r}' - \mathbf{r}_i')\tilde{G}(R)dS' \\ &+ \frac{l_m l_n}{16\pi A_n^+}(\mathbf{r}_m^{c+} - \mathbf{r}_i)\cdot\hat{n}_m \times (\mathbf{r}_m^{c+} - \mathbf{r}_j') \times \iint_{T_n^-}(\mathbf{r}_j' - \mathbf{r}')\tilde{G}(R)dS' \\ &+ \frac{l_m l_n}{16\pi A_n^-}(\mathbf{r}_j - \mathbf{r}_m^{c-})\cdot\hat{n}_m \times (\mathbf{r}_m^{c-} - \mathbf{r}_i') \times \iint_{T_n^+}(\mathbf{r}' - \mathbf{r}_i')\tilde{G}(R)dS' \\ &+ \frac{l_m l_n}{16\pi A_n^-}(\mathbf{r}_j - \mathbf{r}_m^{c-})\cdot\hat{n}_m \times (\mathbf{r}_m^{c-} - \mathbf{r}_j') \times \iint_{T_n^-}(\mathbf{r}_j' - \mathbf{r}')\tilde{G}(R)dS', \end{aligned} \quad (16)$$

where, $\tilde{G}(R) = (jk_0 + \frac{1}{R})\frac{e^{-jk_0R}}{R^2}$.

The remaining source integrals about $\mathbf{r}'$ in the above equations can be calculated with the following nine-point integration method.

C. Barycentric subdivision method for numerical integration

We can apply the barycentric subdivision method (the nine-point quadrature) to the source integral in Eq. (6) and Eq. (16). Each edge of a triangle is equally partitioned into three parts to construct small triangles as shown in Fig. 3, and the small circle "∘" in the figure represents the barycenter of the triangle element.

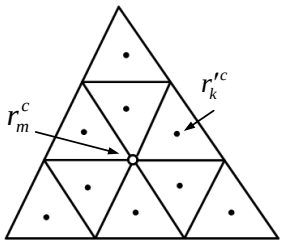

Fig. 3. Nine-point subdivision of a triangle element, where the small circle "∘" denotes the barycenter of the triangle element, "." denotes the barycenter of the sub-triangle elements.

Each triangle is divided into nine equal-sized sub-triangles as shown in Fig. 3. The source integral of the patch can then be approximated by the nine sub-triangles with the same weights. Since these nine triangles have the same area, the integral can be written as:

$$\iint_{T_n} G(\mathbf{r},\mathbf{r}')dS' = \frac{A_n}{9}\sum_{k=1}^{9} G(\mathbf{r},\mathbf{r}'^c_k), \quad (17)$$

By using similar process, the integral in MFIE can be written as:

$$\iint_{T_n}(\mathbf{r}' - \mathbf{r}_\mathbf{i})\tilde{G}(\mathbf{r},\mathbf{r}')dS' = \frac{A_n}{9}\sum_{k=1}^{9}(\mathbf{r}_k'^c - \mathbf{r}_\mathbf{i})\tilde{G}(\mathbf{r},\mathbf{r}_k'^c), \quad (18)$$

where $\mathbf{r}'^c_k$ denotes the quadrature points shown as Fig. 3. The quadrature point of the field integral resides on the barycenter of the patch (triangle), so the quadrature point of the field integral will not coincide with the one of the source integral. Therefore, the value of the integrand will not become singular.

III. NUMERICAL EXAMPLES

A. Computation of radar cross section (RCS)

Case 1: We consider the plane wave scattering of a PEC sphere with radius of 1*m*. We use the Mie series result as benchmark. The incident plane wave has frequency of 300MHz, ϕ^{inc}=0°, θ^{inc}=90°, and vertical polarization. The surface current is computed using the nine-point numerical integration method. The bistatic RCS with VV polarization (vertical polarization excitation and vertical polarization reception) is computed with EFIE and MFIE respectively when the observation angle at ϕ=0° and $\theta \in$ [0°, 180°]. In the computation, the current on the sphere is partitioned into 4527 unknowns.

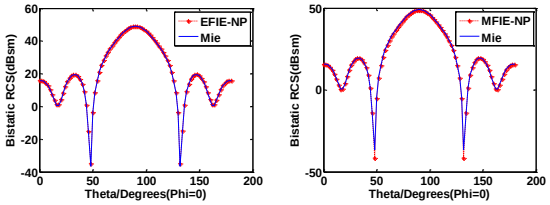

(a) (b)

Fig. 4. The calculation on bistatic RCS: (a) bistatic RCS for PEC sphere solved by EFIE, and (b) bistatic RCS for PEC sphere solved by MFIE.

From Fig. 4 (a) and Fig. 4 (b), we can see that the numerical results have a good agreement with the Mie series results [17, 18, 20]. We can also see that the proposed method works not only for the EFIE equation but also for the MFIE equation.

Case 2: In order to further validate the efficiency of this method to other integral equation and structures, a dielectric sphere and a dielectric cube are computed with PMCHWT and FEM-BI equation, respectively.

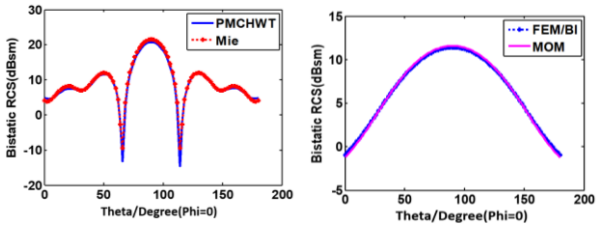

(a) (b)

Fig. 5. Bistatic RCS: (a) dielectric sphere solved by PMCHWT, and (b) dielectric cube solved by FEM-BI.

The dielectric sphere has ε_r=2.5, radius = 1m, the number of unknowns after discretization is 6875. The dielectric cube has ε_r=2.5, side length = 1m, the number of unknowns is 4440. The incident plane wave has the same parameters as Case 1.

From Fig. 5 (a) and Fig. 5 (b), we can see that the numerical results agree well with the Mie series results.

From the above two examples, we can see that this method can be applied to various integration equation and complex structures.

B. Matrix setup time

Using the parameters of Case 1, a comparison of matrix setup time between the nine-point numerical integration and the singularity extraction method is shown in Table 1.

Table 1: Comparison of Matrix setup time

Unknowns	Matrix Setup Time (seconds)	
	Nine-point Numerical Integration	***Singularity Extraction***
1197	10s	17s
4527	2m20s	4m26s
6993	5m45s	10m34s
18297	46m30s	88m12s
50886	367m20s	700m40s

In Table 1, the previous four models are computed on a PC with Intel(R) Core(M) i5-4690K, CPU@3.5GHz/64, RAM 32G, and the last example is a server with Intel(R) Xeon(R) E7-8857v2@3.0GHz, 4 cores, RAM 1.5T.

From Table 1, we can see that the barycentric subdivision method can save nearly half of the setup time compared with the singularity extraction method.

IV. CONVERGENCE ANALYSIS

A. Theory on the barycentric subdivision method

In this section, we will study the convergence of numerical integration using the barycentric subdivision method.

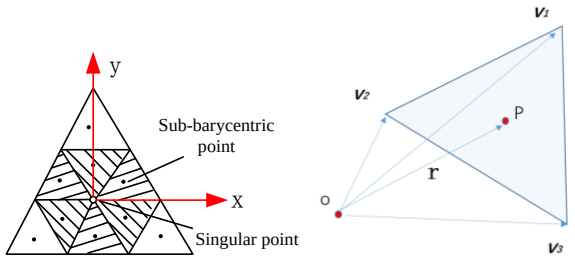

(a) (b)

Fig. 6. Six sub-triangles around the singular point in a triangle element and vector in a sub-triangle. (a) The six small sub-triangles (the shaded area) around the singular point (barycenter of triangle), and (b) the vector for three vertices and quadrature point in a sub-triangle.

The source integral becomes singular when its integration domain overlaps with the field integral. In this case, the source integrals over 6 small triangles around the barycenter "∘" in Fig. 6 (a) will have singularity at one of their corners, i.e. the barycenter"∘" of the triangle.

We can analyze these singular integrals based on the Duffy transform. It transforms from the original barycenter coordinate system (ξ_1,ξ_2,ξ_3) to a new coordinate (u,v), as shown Fig. 6 (b) below (here $\mathbf{v}_1$ is the vector of the singular point"∘"when the field point O is overlapped with $\mathbf{v}_1$):

$$\begin{aligned}\mathbf{r} &= \xi_1\mathbf{v}_1 + \xi_2\mathbf{v}_2 + \xi_3\mathbf{v}_3 \\ &= u\mathbf{v}_1 + v(1-u)\mathbf{v}_2 + (1-v)(1-u)\mathbf{v}_3,\end{aligned} \tag{19}$$

here $\mathbf{v}_1$ is the vector of the singular point, ξ_3=1-ξ_1 –ξ_2, then the singular integral for one sub-triangle can be transformed into:

$$\begin{aligned}I &= \int_S \frac{e^{-jk_0R}}{R}dS = A\int_S \frac{e^{-jk_0|\mathbf{r}-\mathbf{v}_1|}}{|\mathbf{r}-\mathbf{v}_1|}d\xi_1 d\xi_2 \\ &= A\int_0^1\int_0^1 \frac{e^{-jk_0(1-u)|v\mathbf{v}_2+(1-v)\mathbf{v}_3-\mathbf{v}_1|}}{|v\mathbf{v}_2+(1-v)\mathbf{v}_3-\mathbf{v}_1|}dvdu,\end{aligned} \tag{20}$$

where A denotes the area of one sub-triangle S. The integral on S is then converted to a 2-fold integral of u and v, respectively. Now we can define the function $a(v)$:

$$\begin{aligned}a(v) &= k_0\left|v\mathbf{v}_2+(1-v)\mathbf{v}_3-\mathbf{v}_1\right| \\ &= k_0\left|v(\mathbf{v}_2-\mathbf{v}_3)+(\mathbf{v}_3-\mathbf{v}_1)\right|.\end{aligned} \tag{21}$$

From Eq. (21), we can see $a(v)$ is linear with the size of triangle, As the mesh of the target becomes denser, $a(v)$ will be smaller, so the analytical expression I_D of integral I for v is:

$$I_D = A\int_0^1 \frac{dv}{a(v)}\frac{1-e^{-ja(v)}}{ja(v)} \approx Ak_0\int_0^1 \frac{dv}{a(v)}(1+o(a)) = Ak_0/a(\zeta), \tag{22}$$

where $a(\zeta)$ is derived from the mean value theorem for definite integrals [19].

Since the Duffy transformation can eliminate the singularity when the field point overlaps with the singular point as shown in Fig. 6 (a), we can try to eliminate the singularity when the field point at the sub-barycentric point, and further compare these two integral value. The quadrature for the above integral on each sub-triangle samples the domain of integration at (ξ_1,ξ_2) =(1/3,1/3), namely (u,v)=(1/3,1/2) in the new coordinate, substituting the u=1/3, v=1/2 into Eq. (20), the numerical integration on the sub-barycentric point is:

$$I_c \approx Ak_0/a(1/2). \tag{23}$$

The numerical difference between I_D (based on Duffy transform at the singular point) and I_c (based on Duffy transform at the sub-barycentric point) is:

$$I_D - I_c \approx Ak_0\left[1/a(\zeta) - 1/a(1/2)\right]. \tag{24}$$

This difference is only related to the area A. When the area A of triangle tends to zero, the numerical difference $I_D - I_c$ will converge to zero as well. This can ensure that the error is only related to the mesh density,

and convergence of the integral has a good agreement with the traditional Duffy method.

B. Convergence analysis based on numerical experiments

To verify the convergence of the barycentric subdivision method, we compute the bistatic RCS for a PEC sphere with EFIE and MFIE, respectively.

We compute the RCS with the nine-point method and traditional singularity extraction method (S-E) respectively. These two method are compared with Mie series results respectively. The results are shown in Fig. 7.

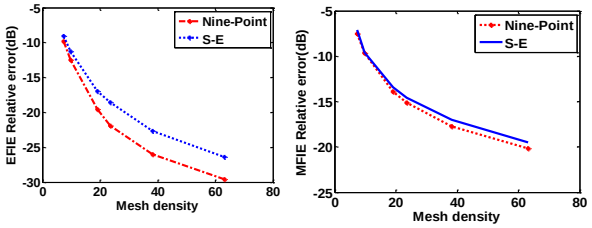

(a) (b)

Fig. 7. Comparison of relative error in RCS. (a) EFIE and (b) MFIE.

The relative error is defined as:

$$error = 10\log\left(\left\|RCS_{\_cal} - RCS_{\_mie}\right\| / \left\|RCS_{\_mie}\right\|\right), \quad (25)$$

and the mesh density is defined as:

$$\text{mesh density} = \sqrt{\frac{N}{S}} \cdot \lambda, \quad (26)$$

where N denotes the numbers of unknowns, S denotes the surface area of the sphere, and λ denotes the wave length of the incident wave. From Fig. 7, we can observe that the error decreases as the mesh density increases.

C. Computation of integrals of 1/R

To check the convergence, we also study the singular integration on a triangle as the below:

$$I = \oiint_{S_m}\left[\oiint_{S_n}(1/R)dS'\right]dS, \quad (27)$$

where R denotes the distance between the source and field point.

In Fig. 8, the size of the area zooms step by step, and the side length L declines by half every time. The value of integration for Eq. (27) is shown in Table 2.

It can be seen from Table 2 that the results of the nine-point method agree well with those of the analytical method. Besides, the two methods diverge at the same time when the area of the triangle becomes too small due to the limited machine precision. In summary, this illustrates that our method is applicable to the cases where the mesh size is small enough.

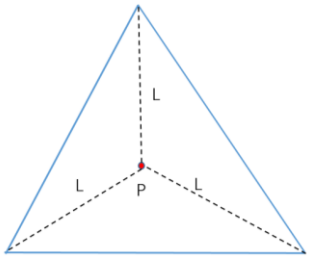

Fig. 8. The area of the triangle changes with L.

Table 2: Comparison of integral value

The Size of Area (L)	The Value of Integral for 1/R	
	The Nine-point	Analytical
1	4.218747139	5.132335663
0.5	0.527344286	0.641542614
0.25	6.59E-02	8.02E-02
0.125	8.24E-03	1.00E-02
0.125/2	1.03E-03	1.25E-03
0.125/2/2	1.29E-04	1.57E-04
0.125/2/2/2	1.61E-05	1.96E-05
0.125/2/2/2/2	2.01E-06	2.45E-06
0.125/2/2/2/2/2	2.51E-07	3.06E-07
0.5/2/2/2/2/2/2/1000	2.17E-16	2.64E-16
0.5/2/2/2/2/2/2/1000/2	NaN	NaN

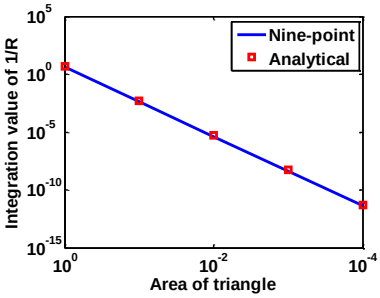

Fig. 9. Convergence for 1/R

The above integral is computed by both the nine-point integration and the analytical method [1], respectively. Figure 9 shows the values of I with respect to mesh density using the two methods. They agree well with each other.

V. CONCLUSION

In this study, we investigated the barycentric subdivision method. We studied the numerical convergence of this method for singular integration by both theoretical analysis and numerical examples. We observe that this method converges at the same level of accuracy as other method such as the singularity extraction. This method avoids the complex treatment of singular integrals and allows a uniform procedure for both singular and non-singular integrations in method of

moments. Numerical examples show that this method can reduce the matrix setup time by half. We hope this study could help us to further understand this method and extend its applications in solving 3D scattering problems using method of moments.

ACKNOWLEDGMENT

This work is supported by National Science Foundation of China under contract 61490693 and 61571264, and the National Basic Research Program of China under contract 2013CB329002, and in part by Beijing National Research Center for Information Science and Technology (BNRist), Guangzhou Science and Technology Plan (201804010266), Beijing Innovation Center for Future Chip, and Research Institute of Tsinghua, Pearl River Delta.

REFERENCES

[1] S. M. Rao, D. R. Wilton, and A. W. Glisson, "Electromagnetic scattering by surfaces of arbitrary shape," *IEEE Trans. Antennas and Propagation*, vol. 30, no. 3, pp. 409-418, 1982.

[2] D. R. Wilton, S. M. Rao, A. W. Glisson, D. H. Schaubert, O. M. Al-Bundak, and C. M. Butler, "Potential integrals for uniform and linear source distributions on polygonal and polyhedral domains," *IEEE Trans. Antennas and Propagation*, vol. 32, no. 3, pp. 276-281, 1984.

[3] M. G. Duffy, "Quadrature over a pyramid or cube of integrands with a singularity at a vertex," *SIAM J. Numer. Anal*., vol. 19, no. 6, pp. 1260-1262, 1982.

[4] Y. W. Zhao, Z. P. Nie, J. H. Xu, and S. B. Wu, "Accurate and efficient calculation of singular integrals in Galerkin method with RWG basis functions," *ACTA Electronica Sinica*, vol. 33, no. 6, pp. 1019-1023, 2005.

[5] M. M. Botha, "A family of augmented Duffy transformations for near-singularity cancellation quadrature," *IEEE Trans. Antennas and Propagation*, vol. 61, no. 6, pp. 3123-3134, 2013.

[6] M. A. Khayat and D. R. Wilton, "Numerical evaluation of singular and near-singular potential integrals,"*IEEE Trans. Antennas and Propagation*, vol. 53, no. 10, pp. 3180-3190, 2005.

[7] M. A. Khayat, D. R. Wilton, and P. W. Fink, "An improved transformation and optimized sampling scheme for the numerical evaluation of singular and near-singular potentials," *IEEE Antennas and Wireless Propagation Letters*, vol. 7, pp. 377-380, 2008.

[8] F. Vipiana and D. R. Wilton, et al., "Numerical evaluation via singularity cancellation schemes of near-singular integrals involving the gradient of Helmholtz-type potentials," *IEEE Trans. Antennas and Propagation*, vol. 61, no. 3, pp. 1255-1265, 2013.

[9] B. D. Popovic and B. M. Kolundzija, *Analysis of Metallic Antennas and Scatters*, The Institution of Electrical Engineers, London, pp. 58, 1988.

[10] F. Z. Geng and C. M. Tong, "An efficient method of singular integrals in hybrid basis MoM solutions," *Journal of Air Force Engineering University (N.S.E.)*, vol. 7, no. 3, pp. 65-68, 2006.

[11] C. W. Xiang and C. M. Tong, et al., "Modeling method of reduced dimension for complex targets and application in electromagnetic scattering analysis," *Chinese Journal of Radio Science*, vol. 20, no. 2, pp. 189~192, 2005.

[12] H. G. Wang and Z. P. Nie, et al., "Singularity analysis of the integral equation for three dimension vector fields scattering," *ACTA Electronica Sinica*, vol. 27, no. 12, pp. 68-71, 1999.

[13] Y. H. Hua and J. P. Xu, et al., "Integration singularity reduction by the locally continuous functions used in moment method with EFIE," *Journal of Electronics and Information Technology*, vol. 25, no. 10, pp. 1436-1440, 2003.

[14] J. H. Wu, X. Y. Cao, H. B. Yuan, and J. Gao, "Effective method to solve magnetic field integral equation with method of moment," *Chinese Journal of Radio Science*, vol. 28, no. 5, pp. 974-978, 2013.

[15] Y. Kamen and L. Shirman, "Triangle rendering using adaptive subdivision," *IEEE Computer Graphics and Application*, pp. 95-103, Mar.-Apr. 1998.

[16] S. N. Makarov, *Antenna and EM Modeling with Matlab*. NY: Wiley-Interscience, New York, pp. 128, 2002.

[17] W. C. Chew, E. Michielssen, J. M. Song, and J. M. Jin, *Fast and Efficient Algorithms in Computational Electromagnetics*. MA: Artech House, Boston, 2001.

[18] J. M. Jin, *Theory and Computation of Electromagnetic Fields*. John Wiley & Sons, Inc., Hoboken, New Jersey, USA, 2010.

[19] AdiBen-Israel and R. Gilbert, *Computer-Supported Calculus*. pp. 224-278, Springer-Verlag Wien, 2002.

[20] X. Q. Sheng, J. M. Jin, J. M. Song, C. C. Lu, and W. C. Chew, "On the formulation of hybrid finite-element and boundary-integral methods for 3-D scattering," *IEEE Trans. Antennas and Propagation*, vol. 46, no. 3, pp. 303-311, 1998.

[21] C. W. Xiang, X. W. Dang, M. K. Li, F. Yang, and S. H. Xu, "The application of barycentric subdivision method for numerical integration in method of moments," *2018 IEEE International Conference on Computational Electromagnetics (ICCEM)*, Chengdu, pp. 1-3, 2018.

[22] F. Vipiana and D. R. Wilton, "Optimized numerical evaluation of singular and near-singular potential

integrals involving junction basis functions," *IEEE Trans. Antennas and Propagation*, vol. 59, no. 1, pp. 162-171, 2011.

[23] S. Jarvenpaa, M. Taskinen, and P. Y. Oijala, "Singularity extraction technique for integral equation methods with higher order basis functions on plane triangles and tetrahedral," *Int. J. Numer. Meth. Eng*., vol. 58, pp. 1149-1165, Aug. 2003.

Chunwang Xiang received the B.S. degree from Air Force Engineering University, Xi'an, China, in 2002. He is now a Ph.D. student at Tsinghua University, Beijing, China. His current research interests include finite element method (FEM), time-domain finite element method (FETD), finite element boundary integral method (FE-BI), and design on Radar antenna and etc.

Xunwang Dang received the B.S. degree from Tsinghua University, Beijing, China, in 2013, and the Ph.D. degree from the same university in 2018.

His current research interests include reduced basis method (RBM), equivalent principle algorithm (EPA), fast algorithms in the method of moments, deep learning techniques in electromagnetics etc.

Maokun Li received his B.S. degree in Electronic Engineering from Tsinghua University, Beijing, China, in 2002, and the M.S. and Ph.D. degrees in Electrical Engineering from University of Illinois at Urbana-Champaign in 2004 and 2007, respectively. After graduation, he joined Schlumberger-Doll Research as a Post-doc Research Scientist, and later as a Senior Research Scientist. In June 2014, he joined the Department of Electronic Engineering in Tsinghua University as an Associate Professor. His research interests include fast algorithms in computational electromagnetics and electromagnetic inverse problems.

Fan Yang received the B.S. and M.S. degrees in Electronic Engineering from Tsinghua University, Beijing, China, in 1997 and 1999, respectively, and the Ph.D. degree in Electrical Engineering from the University of California, Los Angeles (UCLA), Los Angeles, CA, USA, in 2002. From 2002 to 2004, he was a Postdoctoral Research Engineer and Instructor with the Electrical Engineering Department, UCLA. In 2004, he joined the Electrical Engineering Department, The University of Mississippi as an Associate Professor in 2009. In 2011, he joined the Electronic Engineering Department, Tsinghua University as a Professor, and has served as the Director of the Microwave and Antenna Institute since then. He has authored or coauthored more than 300 journal articles and conference papers, 6 book chapters, and 5 books. His research interests include antennas, surface electromagnetics, computational electromagnetics and applied electromagnetic systems.

Yang served as an Associate Editor for the IEEE Transactions on Antennas and Propagation (2010–2013) and an Associate Editor-in-Chief for Applied Computational Electromagnetics Society Journal (2008–2014). He was the Technical Program Committee Chair of 2014 IEEE International Symposium on Antennas and Propagation and USNC-URSI Radio Science Meeting. He is a Fellow of IEEE and ACES. He is also an IEEE APS Distinguished Lecturer for 2018–2020.

Shenheng Xu received the B.S. and M.S. degrees in 2001 and 2004, respectively, from the Southeast University, Nanjing, China, and the Ph.D. degree in Electrical Engineering in 2009 from the University of California, Los Angeles (UCLA), CA, USA. From 2000 to 2004, he was a Research Assistant with the State Key Laboratory of Millimeter Waves, Southeast University, Nanjing, China. From 2004 to 2011, he was a Graduate Student Researcher and later a Postdoctoral Researcher with the Antenna Research, Analysis, and Measurement Laboratory, UCLA. In 2012, he joined the Department of Electronic Engineering, Tsinghua University, Beijing, China, as an Associate Professor. His research interests include novel designs of high-gain antennas for advanced applications, artificial electromagnetic structures, and electromagnetic and antenna theories.